Constraining the cosmology of the phantom brane using distance measures

Ujjaini Alam,[1,*] Satadru Bag,[2,†] and Varun Sahni[2,‡]

[1]*Physics & Applied Mathematics Unit, Indian Statistical Institute, Kolkata 700108, India*
[2]*Inter University Center for Astronomy & Astrophysics, Pune 411007, India*

(Received 12 October 2016; published 30 January 2017)

The phantom brane has several important distinctive features: (i) Its equation of state is phantomlike, but there is no future "big rip" singularity, and (ii) the effective cosmological constant on the brane is dynamically screened, because of which the expansion rate is *smaller* than that in ΛCDM at high redshifts. In this paper, we constrain the Phantom braneworld using distance measures such as type-Ia supernovae (SNeIa), baryon acoustic oscillations (BAO), and the compressed cosmic microwave background (CMB) data. We find that the simplest braneworld models provide a good fit to the data. For instance, BAO + SNeIa data can be accommodated by the braneworld for a large region in parameter space $0 \leq \Omega_\ell \lesssim 0.3$ at 1σ. The Hubble parameter can be as high as $H_0 \lesssim 78\ \mathrm{km\,s^{-1}\,Mpc^{-1}}$, and the effective equation of state at present can show phantomlike behavior with $w_0 \lesssim -1.2$ at 1σ. We note a correlation between H_0 and w_0, with higher values of H_0 leading to a lower, and more phantomlike, value of w_0. Inclusion of CMB data provides tighter constraints $\Omega_\ell \lesssim 0.1$. (Here Ω_ℓ encodes the ratio of the five- and four-dimensional Planck mass.) The Hubble parameter in this case is more tightly constrained to $H_0 \lesssim 71\ \mathrm{km\,s^{-1}\,Mpc^{-1}}$, and the effective equation of state to $w_0 \lesssim -1.1$. Interestingly, we find that the Universe is allowed to be closed or open, with $-0.5 \lesssim \Omega_\kappa \lesssim 0.5$, even on including the compressed CMB data. There appears to be some tension in the low and high-z BAO data which may either be resolved by future data, or act as a pointer to interesting new cosmology.

DOI: 10.1103/PhysRevD.95.023524

I. INTRODUCTION

The unexpected faintness of distant supernova type Ia, as observed concurrently by the Supernova Cosmology Project and the High Redshift Search Team [1,2] in the late 1990s, has led to the postulation of one of the most mystifying cosmological phenomena—the accelerated expansion of the Universe. One way to explain this observational result is to theorize the existence of a new form of energy, with negative pressure, often called "dark energy." Many different models have been suggested for this dark energy, some of which are reviewed in [3,4]. Current cosmological observations are commensurate with the cosmological constant [5], where the dark energy equation of state is -1 and its energy density is constant. However, other dark energy models are by no means ruled out [6], and the search for the true nature of dark energy is a continuing process.

A different approach to the problem of cosmological acceleration consists of introducing new physics in the gravitational sector. Einsteinian gravity is very well tested within the Solar System, but may be modified on larger scales. Different models of modified gravity have been suggested to explain the accelerated expansion of the Universe [7], including $f(R)$ models, galileons etc. We consider here a braneworld scenario, where our observable Universe is situated in a four-dimensional brane embedded in a fifth dimension, the "bulk," and the accelerated expansion of the Universe is a consequence of this modification of gravity. Braneworld scenarios could have important cosmological consequences. For instance, (i) the Randall-Sundrum (RS) model [8], which modifies gravity at small scales, could potentially explain the galaxy rotation curves in lieu of dark matter [9]; (ii) an RS-type braneworld, but with a timelike extra dimension, makes the Universe bounce at early times, alleviating thereby the big bang singularity [10]. The braneworld models which produce accelerated expansion of the Universe tend to modify gravity on large scales. An early example, the Dvali Gabadadze Porrati Model, was constructed in [11] while a more general braneworld model containing the induced gravity term as well as cosmological constants in the bulk and on the brane, has been studied in [12–15].

In this work we study a braneworld model for the accelerated expansion of the Universe that was introduced in [15] and discussed in greater detail in [16,17]. We revisit this model in the context of observations of the cosmological distance and attempt to constrain it from the latest data. In the following sections, we first define our braneworld model in Sec. II, discuss the data and methodology in Sec. III, show the results of our analysis in Sec. IV, and present our conclusions in Sec. V.

*ujjaini.alam@gmail.com
†satadru@iucaa.in
‡varun@iucaa.in

II. COSMOLOGICAL EVOLUTION OF THE BRANEWORLD MODEL

We consider a braneworld scenario where the equations of motion are derived from the action [15]

$$S = M^3\left[\int_{\rm bulk}(R_5 - 2\Lambda_b) - 2\int_{\rm brane} K\right] + \int_{\rm brane}(m^2 R_4 - 2\sigma) + \int_{\rm brane} L(h_{\alpha\beta},\phi), \quad (1)$$

where R_5 is the scalar curvature of the metric g_{ab} in the five-dimensional bulk, and R_4 is the scalar curvature of the induced metric $h_{\alpha\beta}$ on the brane. The quantity $K = K_{\alpha\beta}h^{\alpha\beta}$ is the trace of the extrinsic curvature $K_{\alpha\beta}$ on the brane defined with respect to its inner normal. $L(h_{\alpha\beta},\phi)$ is the four-dimensional matter field Lagrangian, M and m denote, respectively, the five-dimensional and four-dimensional Planck masses, Λ_b is the bulk cosmological constant, and σ is the brane tension. Integrations in Eq. (1) are performed with respect to the natural volume elements on the bulk and brane. The presence of the brane curvature term $m^2\int_{\rm brane} R_4$ in Eq. (1) introduces the length scale $\ell = 2m^2/M^3$. On short length scales $r \ll \ell$ (early times) one recovers general relativity, whereas on large length scales $r \gg \ell$ (late times) brane-specific effects begin to play an important role, leading to the acceleration of the Universe at late times.

The cosmological evolution of the braneworld is described by the Hubble parameter

$$H^2 + \frac{\kappa}{a^2} = \frac{\rho+\sigma}{3m^2} + \underline{\frac{2}{\ell^2}\left[1 \pm \sqrt{1 + \ell^2\left(\frac{\rho+\sigma}{3m^2} - \frac{\Lambda_b}{6} - \frac{C}{a^4}\right)}\right]}, \qquad m^2 = \frac{1}{8\pi G}, \quad (2)$$

where $H = \dot{a}/a$ is the Hubble parameter, $\rho = \rho(t)$ is the energy density of matter and radiation on the brane, C/a^4 represents the dark radiation term and κ, the curvature of the Universe. The underlined terms make the braneworld models different from standard Friedmann-Lemaître-Robertson-Walker cosmology. The $\pm$ signs in Eq. (2) correspond to the two separate ways in which the brane can be embedded in the higher dimensional bulk. The two signs represent two branches of cosmological solutions, the $+$ sign denoting the "self-accelerating" branch which can model late-time acceleration without cosmological constant in the bulk or on the brane, while the $-$ sign represents the normal branch where at least a brane tension is required to accelerate the expansion. It has been shown that the self-accelerating branch is plagued by ghost instability issues at least in the DGP model of braneworlds [18]. In this paper, we limit ourselves to the the $-$ sign, or the normal branch, which exhibits phantomlike behavior. A version of this model has been previously studied in the context of an older data set in [19], and we now extend this analysis for the newest data using all the different braneworld parameters.

The reduced Hubble parameter $h(z) = H(z)/H_0$ can be calculated from (2) to be

$$h^2(z) = \Omega_{0r}(1+z)^4 + \Omega_{0m}(1+z)^3 + \Omega_\kappa(1+z)^2 + \Omega_\sigma + 2\Omega_\ell - 2\sqrt{\Omega_\ell}\sqrt{\Omega_{0r}(1+z)^4 + \Omega_{0m}(1+z)^3 + \Omega_\sigma + \Omega_\ell + \Omega_{\Lambda_b} + \Omega_C(1+z)^4}, \quad (3)$$

with the additional constraint relation

$$\Omega_\sigma = 1 - \Omega_{0r} - \Omega_{0m} - \Omega_\kappa + 2\sqrt{\Omega_\ell}\sqrt{1 + \Omega_{\Lambda_b} + \Omega_C - \Omega_\kappa}. \quad (4)$$

Here

$$\Omega_{0m} = \frac{\rho_{0m}}{3m^2H_0^2}, \quad \Omega_{0r} = \frac{\rho_{0r}}{3m^2H_0^2}, \quad \Omega_\kappa = -\frac{\kappa}{a_0^2H_0^2}, \quad \Omega_\sigma = \frac{\sigma}{3m^2H_0^2}, \quad \Omega_\ell = \frac{1}{\ell^2H_0^2}, \quad \Omega_{\Lambda_b} = -\frac{\Lambda_b}{6H_0^2}, \quad \Omega_C = -\frac{C}{a_0^4H_0^2} \quad (5)$$

are dimensionless parameters. In the limit $\Omega_\ell \to 0$, the braneworld reduces to the ΛCDM model. The parameters to be constrained are Ω_{0m}, Ω_ℓ, Ω_{Λ_b}, Ω_κ, Ω_C and H_0 [Ω_σ is constrained by Eq. (4)]. The value of the radiation density can be calculated from the cosmic microwave background (CMB) temperature or from big bang nucleosynthesis (BBN) considerations to a high degree of accuracy.

A simpler variant of the above model is obtained by setting $\Omega_\kappa = \Omega_C = \Omega_{\Lambda_b} = 0$ and neglecting the presence of radiation at low redshifts. In this case (3) and (4) reduce to

$$h^2(z) = \Omega_{0m}(1+z)^3 + \Omega_\sigma + 2\Omega_\ell - 2\sqrt{\Omega_\ell}\sqrt{\Omega_{0m}(1+z)^3 + \Omega_\sigma + \Omega_\ell}, \quad (6)$$

$$\Omega_\sigma = 1 - \Omega_{0m} + 2\sqrt{\Omega_\ell}. \quad (7)$$

This model has several interesting features which hold for the entire normal-branch Braneworld family.

(1) First and foremost is the fact that the current value of the effective equation of state is phantomlike, i.e., $w_{\rm eff} < -1$. To appreciate this let us define the energy density and pressure of dark energy on the brane as follows [4],

$$\rho_{\rm DE} = \frac{3H^2}{8\pi G}(1-\Omega_m),$$
$$p_{\rm DE} = \frac{H^2}{4\pi G}\left(q-\frac{1}{2}\right), \tag{8}$$

where

$$q \equiv -\ddot{a}/aH^2 = x\frac{H'(x)}{H(x)} - 1, \qquad x = 1+z, \tag{9}$$

is the deceleration parameter (the prime denotes differentiation with respect to x or z) and Ω_m is the total density of nonrelativistic matter in terms of its critical value

$$\Omega_m(z) = \frac{\Omega_{0m}(1+z)^3}{h^2(z)}. \tag{10}$$

The effective equation of state (EOS) of dark energy, $w_{\rm eff} = p_{\rm DE}/\rho_{\rm DE}$, is then given by

$$w_{\rm eff}(z) = \frac{2q(z)-1}{3(1-\Omega_m(z))}. \tag{11}$$

Substituting from (9), (10) and (6) into (11) we get $w_{\rm eff}(z)$ for the Phantom braneworld as

$$w_{\rm eff}(z) = -1 - \frac{\Omega_m(z)}{1-\Omega_m(z)} \times \sqrt{\frac{\Omega_\ell}{\Omega_{0m}(1+z)^3+\Omega_\sigma+\Omega_\ell}}. \tag{12}$$

At the present epoch ($z=0$),

$$w_0 \equiv w_{\rm eff}(z=0) = -1 - \frac{\Omega_{0m}}{1-\Omega_{0m}}\left(\frac{\sqrt{\Omega_\ell}}{1+\sqrt{\Omega_\ell}}\right), \tag{13}$$

demonstrating that the present value of the effective equation of state of the dark energy is *phantomlike*, i.e. $w_0 < -1$. Figure 1 shows w_0 as a function of Ω_ℓ. We find that $w_0 \to -1/(1-\Omega_{0m})$ asymptotically, as $\Omega_\ell \to \infty$.

(2) A second important feature of the phantom brane is that the effective cosmological constant on the brane can be *screened*. This can easily be seen by rewriting (6) in the more suggestive form

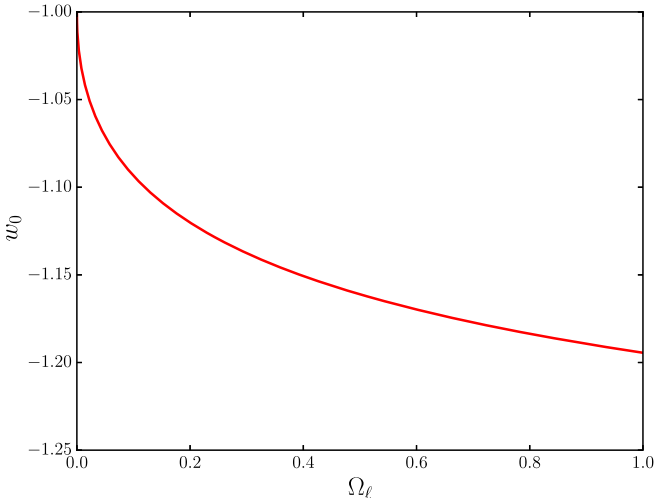

FIG. 1. The current value of the effective equation of state of dark energy (w_0) in the braneworld model (16) is shown as a function of Ω_ℓ ($\Omega_{0m} = 0.28$ is assumed). For $\Omega_\ell \to 0$, one recovers ΛCDM limit.

$$h^2(z) = \Omega_{0m}(1+z)^3 + \Omega_\Lambda - f(z) \tag{14}$$

where $\Omega_\Lambda = \Omega_\sigma + 2\Omega_\ell$ and $f(z)$ is the screening term $f(z) = -2\sqrt{\Omega_\ell}\sqrt{\Omega_{0m}(1+z)^3+\Omega_\sigma+\Omega_\ell}$ whose value *increases* with redshift. The presence of this term permits the expansion rate to *fall below* the ΛCDM value of $h^2(z) = \Omega_{0m}(1+z)^3 + \Omega_\Lambda$ at high redshifts [6,15,20]. The screening mechanism, operational in the braneworld,[1] can potentially be tested by observations of $h(z)$. As pointed out in [6], the phantom brane may provide a better fit to high-z baryon acoustic oscillations (BAO) data than ΛCDM. Future BAO data are likely to improve on this result by providing very accurate measurements of the expansion history of the Universe. Combining observations of $h(z)$ with the Om diagnostic [6,22], and eventually with the Statefinder [23], would allow one to assess the nature of dark energy in a model-independent manner [24].

As noted in [6], a key feature of screened dark energy models is that if $f(z)$ increases monotonically with redshift, then eventually the cosmological constant, Ω_Λ, is canceled by $f(z)$, so that $h^2(z_p) = \Omega_{0m}(1+z_p)^3$. At this redshift, z_p, the effective equation of state of dark energy develops a pole at which $w_{\rm eff}(z_p) \to \infty$ [6,16]. In the context of the phantom brane, the pole in $w_{\rm eff}(z)$ is shown in Fig. 2. It is easy to see that the presence of the pole is generic and arises when $\Omega_m(z_p) = 1$ in the

[1]The cosmological constant can also be dynamically screened in other cosmological scenarios, some of which are discussed in [21].

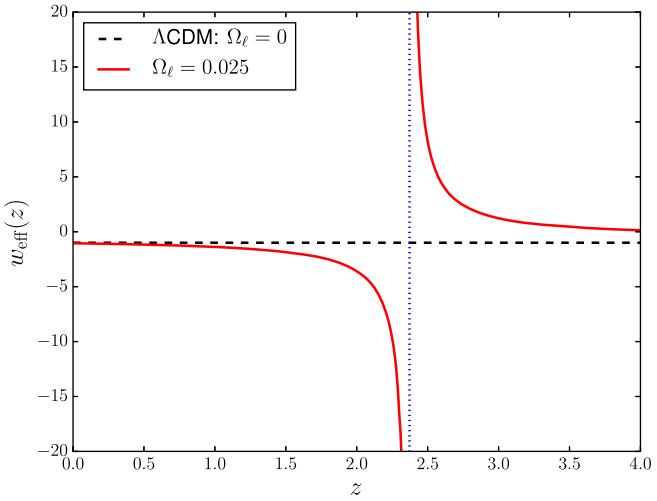

FIG. 2. The effective equation of state of dark energy ($w_{\rm eff}$) is shown as a function of redshift for $\Omega_\ell = 0.025$, assuming $\Omega_{0m} = 0.28$. A pole occurs at $z_p \approx 2.372$. At large redshift, $w_{\rm eff}(z) \to -1/2$ for any nonzero value of Ω_ℓ and Ω_{0m}. For $\Omega_\ell = 0$, i.e. in the ΛCDM limit, the pole disappears as shown by the dashed line.

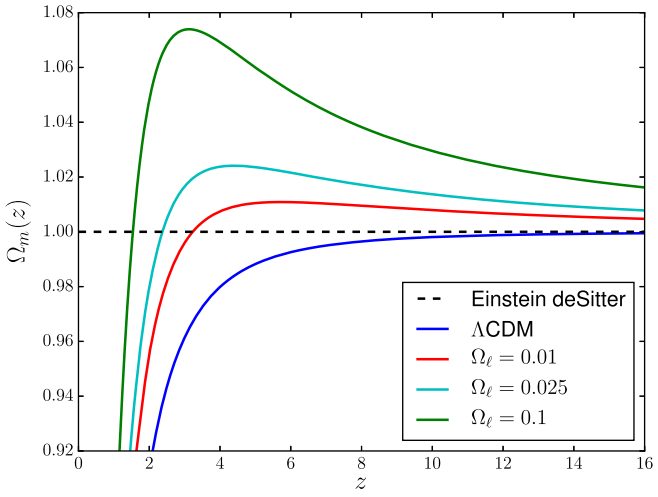

FIG. 3. $\Omega_m(z)$, given by (10), is plotted against the redshift z for various Ω_ℓ, assuming $\Omega_{0m} = 0.28$. During matter domination (large z), $\Omega_m(z)$ approaches unity. In the phantom braneworld $\Omega_m(z)$ possesses a maximum and $\Omega_m(z) > 1$ while $z > z_p$. The pole in $w_{\rm eff}(z)$ occurs at $z = z_p$ when $\Omega_m(z_p) = 1$. As Ω_ℓ increases, $\Omega_m(z)$ becomes unity at lower redshift, i.e. z_p decreases, which is explicitly shown in Fig. 4. For Einstein de Sitter universe $\Omega_m(z) = 1$ always.

denominator of (12). Actually $\Omega_m(z)$ in the phantom braneworld possesses a maximum and remains greater than unity for $z > z_p$, as shown in Fig. 3. This figure informs us that, for increasing values of Ω_ℓ, $\Omega_m(z)$ reaches unity at lower redshifts. This implies that z_p decreases with increasing Ω_ℓ. The redshift of the pole, z_p, is given by

$$(1 + z_p)^3 = \frac{\Omega_\sigma^2}{4\Omega_{0m}\Omega_\ell}. \tag{15}$$

The value of z_p is plotted against Ω_ℓ in Fig. 4. Using the closure relation (17), we find that $(1 + z_p)^3 \to 1/\Omega_{0m}$ asymptotically as $\Omega_\ell \to \infty$. The presence of a pole in the EOS of dark energy therefore emerges as a *smoking gun* test for this class of braneworld models. We note that such a pole may also be present for other dark energy models in which the dark energy density crosses 0.

The above characteristics for this subset of phantom brane also hold true for other subsets of this model which are considered in this work.

(i) Our base braneworld model is a flat universe without dark radiation, i.e., $\kappa = 0$, $C = 0$. This is very similar to the simplest variant for the phantom brane considered above, except that the radiation density is explicitly considered as well, since high redshift data are also considered. The reduced Hubble parameter has the form

$$h^2(z) = \Omega_{0r}(1+z)^4 + \Omega_{0m}(1+z)^3 + \Omega_\sigma + 2\Omega_\ell - 2\sqrt{\Omega_\ell}\sqrt{\Omega_{0r}(1+z)^4 + \Omega_{0m}(1+z)^3 + \Omega_\sigma + \Omega_\ell + \Omega_{\Lambda_b}}, \tag{16}$$

with the additional constraint relation

$$\Omega_\sigma = 1 - \Omega_{0r} - \Omega_{0m} + 2\sqrt{\Omega_\ell}\sqrt{1 + \Omega_{\Lambda_b}}. \tag{17}$$

The effective equation of state at present is given by

$$w_0 = -1 - \frac{1}{3}\frac{\sqrt{\Omega_\ell}(4\Omega_{0r} + 3\Omega_{0m})}{(1 - \Omega_{0r} - \Omega_{0m})(\sqrt{1 + \Omega_{\Lambda_b}} + \sqrt{\Omega_\ell})}. \tag{18}$$

The parameters to be fitted are Ω_{0m}, Ω_ℓ, Ω_{Λ_b} and H_0.

(ii) We also study the phantom brane including dark radiation as a parameter, in a flat universe, i.e., $\kappa = 0$, $C \neq 0$. The reduced Hubble parameter is therefore given by

$$h^2(z) = \Omega_{0r}(1+z)^4 + \Omega_{0m}(1+z)^3 + \Omega_\sigma + 2\Omega_\ell - 2\sqrt{\Omega_\ell}\sqrt{\Omega_{0r}(1+z)^4 + \Omega_{0m}(1+z)^3 + \Omega_C(1+z)^4 + \Omega_\sigma + \Omega_\ell + \Omega_{\Lambda_b}}, \tag{19}$$

with the additional constraint relation

$$\Omega_\sigma = 1 - \Omega_{0r} - \Omega_{0m} + 2\sqrt{\Omega_\ell}\sqrt{1 + \Omega_{\Lambda_b} + \Omega_C}. \tag{20}$$

Here the effective equation of state at present takes the form

$$w_0 = -1 - \frac{1}{3}\frac{\sqrt{\Omega_\ell}(4\Omega_{0r} + 3\Omega_{0m} + 4\Omega_C)}{(1 - \Omega_{0r} - \Omega_{0m})(\sqrt{1 + \Omega_{\Lambda_b} + \Omega_C} + \sqrt{\Omega_\ell})}. \tag{21}$$

The parameters to be fitted are Ω_{0m}, Ω_ℓ, Ω_{Λ_b}, Ω_C and H_0. The dark radiation term appears to act almost like a curvature term.

(iii) We free up the curvature of space, but exclude dark radiation, i.e., $\kappa \neq 0$, $C = 0$. In this case, the reduced Hubble parameter is given by

$$h^2(z) = \Omega_{0r}(1+z)^4 + \Omega_{0m}(1+z)^3 + \Omega_\kappa(1+z)^2 + \Omega_\sigma + 2\Omega_\ell - 2\sqrt{\Omega_\ell}\sqrt{\Omega_{0r}(1+z)^4 + \Omega_{0m}(1+z)^3 + \Omega_\sigma + \Omega_\ell + \Omega_{\Lambda_b}}, \tag{22}$$

with the additional constraint relation

$$\Omega_\sigma = 1 - \Omega_{0r} - \Omega_{0m} - \Omega_\kappa + 2\sqrt{\Omega_\ell}\sqrt{1 + \Omega_{\Lambda_b} - \Omega_\kappa}. \tag{23}$$

The effective equation of state at present is now given by

$$w_0 = -1 - \frac{1}{3}\frac{\sqrt{\Omega_\ell}(4\Omega_{0r} + 3\Omega_{0m})}{(1 - \Omega_{0r} - \Omega_{0m} - \Omega_\kappa)(\sqrt{1 + \Omega_{\Lambda_b} - \Omega_\kappa} + \sqrt{\Omega_\ell})}. \tag{24}$$

The parameters to be fitted are Ω_{0m}, Ω_ℓ, Ω_{Λ_b}, Ω_κ and H_0. Current CMB measurements show that the Universe is practically flat, with $\Omega_\kappa \sim 0$, for the cosmological constant, as we see this strong constraint may not hold in the braneworld scenario.

It is possible to consider a model including both the dark radiation and curvature terms, but since both terms have a similar effect on the expansion of the Universe [both being proportional to $\sim(1+z)^2$], we expect them to be somewhat degenerate with each other, so it would not be possible to easily discriminate them using distance measures alone.

III. DATA AND METHODOLOGY

We use here the cosmological data that give quasimodel-independent information on the background expansion of the Universe. The most commonly used data for this purpose are the supernova type Ia [25,26]. There are also the baryon acoustic oscillations [27–29], the comoving size of the sound horizon at last scattering surface from CMB data [5], the value of the Hubble parameter derived from various independent sources [30], gamma ray bursts [31], direct measurements of the Hubble constant H_0 [32–34] etc.

Not all the data are regarded with the same degree of confidence, e.g., the gamma ray burst observations meet with some scepticism from the community due to the large scatter in their intrinsic properties. We therefore choose not to utilize these data in our analysis.

Direct measurements of H_0 are also subject to various tensions. The HST Cepheid + supernovae (SNe)-based estimate from [32] gives $H_0 = (73.8 \pm 2.4)\,\mathrm{km\,s^{-1}\,Mpc^{-1}}$. The same Cepheid data have been reanalyzed in [33] using revised geometric maser distance to NGC 4258. Using NGC 4258 as a distance anchor, they find $H_0 = (70.6 \pm 3.3)\,\mathrm{km\,s^{-1}\,Mpc^{-1}}$. A recent paper, [34], obtains a 2.4% determination of the Hubble constant at $H_0 = 73.24 \pm 1.74\,\mathrm{km\,s^{-1}\,Mpc^{-1}}$ combining the anchor NGC

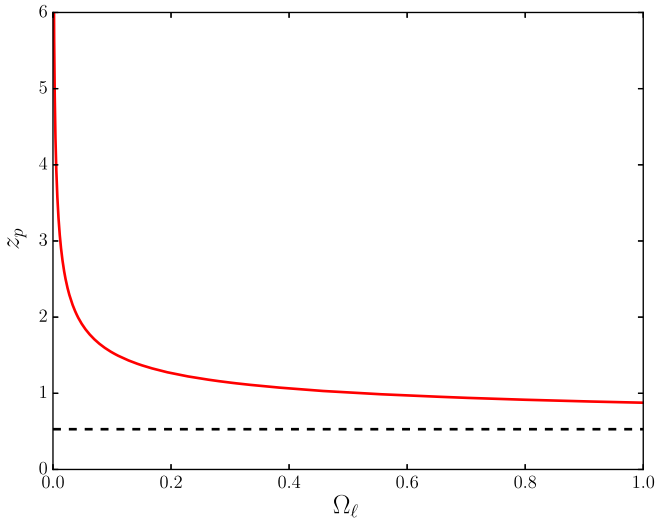

FIG. 4. The redshift of the pole in $w_{\rm eff}(z)$ is shown as a function of Ω_{ℓ}. The dashed line corresponds to the asymptotic value of z_p: $z_p \to [(1/\Omega_{0m})^{1/3} - 1]$ for $\Omega_{\ell} \to \infty$. For $\Omega_{0m} = 0.28$ the asymptote is at $z_p \approx 0.53$.

4258, Milky Way and LMC Cepheids. This value disagrees at 3σ with that predicted by Planck for the ΛCDM three-neutrino model in [5], which is $H_0 = 67.3 \pm 1.0\ {\rm km\,s^{-1}\,Mpc^{-1}}$. The Milky Way Cepheid solutions for H_0 may be unstable [33], which could go some way in explaining this inconsistency. Recent strong lensing observations, [35], give the value $H_0 = 71.9^{+2.4}_{-3.0}\ {\rm km\,s^{-1}\,Mpc^{-1}}$. On the other hand, the Planck results appear to favor a lower value of H_0 [5]. Hubble parameter measurements from SNe and red giant halo populations [36] give $H_0 = 63.7 \pm 2.3\ {\rm km\,s^{-1}\,Mpc^{-1}}$. A recent Hubble parameter measurement by [37] prefers a value of $H_0 = 68.3^{+2.7}_{-2.6}\ {\rm km\,s^{-1}\,Mpc^{-1}}$. The most recent Sloan Digital Sky Survey DR12 BAO data [29] also appear to favor a somewhat low value of $H_0 = 67.8 \pm 1.2\ {\rm km\,s^{-1}\,Mpc^{-1}}$. Historically, direct measurements of H_0 have often resulted in widely discrepant values. Even today, some measurements find comparatively higher values of H_0 than others. There are also issues with the reliability of analysis for the different data sets. In our analysis, we do not use any priors on H_0 and let the analysis choose the preferred value of H_0.

The cosmic chronometer data sets, which estimate the Hubble parameter with different evolution of cosmic chronometers in the redshift range $0 < z < 2$, have been recently used in [38] to constrain the equation of state. These data sets may be somewhat dependent on the assumptions of evolutionary stellar population synthesis models; they also rely on the correct identification of tracers and reliable age dating. The constraints obtained from these data sets in conjunction with other data appear to favor phantom behavior over $w > -1$ models; therefore these data sets may well fit our phantom braneworld models successfully. For the moment we leave this data set out, since the assumption dependence of these data sets is still being studied.

We create here a base data set comprising those observations whose systematics are well constrained, or which have already been used with some success in conjunction with each other.

A. Supernova data

We use the Union2.1 type-Ia supernovae (SNeIa) data set [25] comprising 580 SNe between $z \sim 0.01$ and 1.4, with average errors $\sigma_\mu \sim 0.1$–0.6. One can also use the JLA data set [26] which combines the SNLS and SDSS SNe to create an extended sample of 740 SNe, with apparently better calibration quality, but this does not appreciably change results. We use the full SNe error covariance matrices for the analysis. The data are in the form

$$\mu(z) = 5\log_{10}\left(\frac{c(1+z)}{H_0}\int_0^z \frac{dz}{h(z)}\right), \tag{25}$$

with $h(z)$ given by Eq. (3). It should be noted that at the redshifts considered, the radiation density is negligible, and that the only effect of the parameter H_0 is as an additive constant. Thus marginalizing over H_0 does not affect the SNe results.

B. BAO data

The current BAO data may be divided into the low redshift galaxy BAO data, and the higher redshift Lyα data (see Table I, following [27] and [29]). The low redshift data typically measure a combination of the angular diameter

TABLE I. BAO data from different surveys. The two high-z Lyα points have a distinct character to the low redshift data, and the data are often divided into two sets—low redshift galaxy BAO data and high redshift Lyα data.

Source	z	D_V/r_d	σ	D_M/r_d	σ	D_H/r_d	σ
6dFGS	0.106	3.047	0.137	⋯	⋯	⋯	⋯
SDSS-MGS	0.15	4.480	0.168	⋯	⋯	⋯	⋯
BOSS-LOWz	0.32	8.594	0.095	8.774	0.142	25.89	0.76
BOSS-CMASS	0.57	13.757	0.142	14.745	0.237	21.02	0.52
LyaFauto	2.34	⋯	⋯	37.675	2.171	9.18	0.28
LyaF-QSOcross	2.36	⋯	⋯	36.288	1.344	9.00	0.30

distance and the Hubble parameter, while the BOSS survey is able to get separate measurements on both the angular diameter distance and the Hubble parameter. For the galaxy data, we use the latest SDSS 12th data release [29], while for the high redshift Lyα data we use the SDSS 11th data release [28], since the 12th release is not yet available for these. In their most model-independent form, the observations are presented as a ratio of the distance between measure (D_M, D_H, D_V) and the quantity r_d, which is the comoving sound horizon at the end of the baryon drag epoch. Therefore the quantities measured model independently are D_V/r_d, D_M/r_d, D_H/r_d, which are given by

$$r_d = \frac{1}{H_0}\int_{z_d}^{\infty}\frac{c_s(z)dz}{h(z)}; \quad c_s(z) = \frac{c}{\sqrt{3}\sqrt{1+0.75\frac{\Omega_{0b}h^2}{\Omega_{0\gamma}h^2(1+z)}}}, \tag{26}$$

$$D_H(z) = \frac{c}{H_0 h(z)}, \tag{27}$$

$$D_M(z) = \frac{c}{H_0}\int_0^z \frac{dz}{h(z)}, \tag{28}$$

$$D_V(z) = [zD_H(z)D_M^2(z)]^{1/3}, \tag{29}$$

where $h = H_0/100$, Ω_{0b} is the baryon energy density, and $\Omega_{0\gamma}$ is the photon energy density. Typically, for the observations where D_M, D_H are available separately, we use these directly, taking into account the covariance between them. Where separately measurements are not available (6dFGS and SDSS-MGS), we use the combination of these two, i.e., D_V.

There are two points to note in the above equations. First, in r_d, we have the sound speed $c_s(z)$ which depends on the ratio of baryon energy density and photon energy density. We may input $\Omega_{0b}h^2$ from BBN considerations and $\Omega_{0\gamma}h^2$ from CMB temperature using the standard scenario, which are both independent of braneworld parameters or other cosmological parameters except the radiation era physics.

Secondly, note that, due to the ratios taken, the quantity $h = H_0/100$ does not appear as a multiplicative or additive in the BAO data. It only appears inside $h(z)$, as part of the radiation term, since the CMB constraint on this term is on $\Omega_{0\gamma}h^2$, rather than on $\Omega_{0\gamma}$. For all the quantities at low z, the effect of the radiation term is negligible, as in the SNe data; however, for the drag distance, r_d, it is significant and neglecting the radiation term for r_d leads to erroneous results. One can assume the r_d obtained from Planck, or use an approximation for it, however, since these are usually obtained for ΛCDM with typical values of Ω_{0m}, h etc., so in an analysis where both Ω_{0m} and h are parameters, this could change/bias the results by several percent. See Fig. 5 for some illustrative examples of the variation in r_d with Ω_{0m} and h (the braneworld parameters are not relevant at these early times).

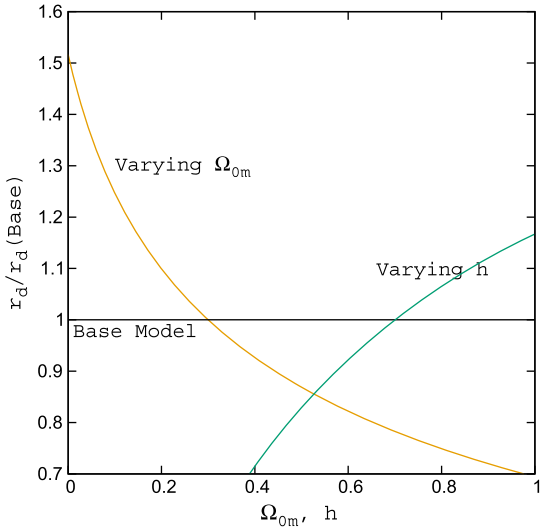

FIG. 5. Variation of r_d with h, Ω_{0m}. The black line represents the base model with $\Omega_{0m} = 0.3$, $h = 0.7$, $\Omega_{\ell'} = \Omega_{\Lambda_b} = 0$; the orange line represents the variation of r_d with Ω_{0m}, and the green line represents the variation of r_d with h.

Therefore the correct way to deal with this term is to calculate it analytically at each step, for each value of Ω_{0m}, and marginalize over h. We assume the Planck value for the drag redshift $z_d = 1059.68$ for this, as we do not expect that z_d is as sensitive to the cosmology as r_d.

We also note here that, when interpreting the BAO results in the framework of braneworlds, we implicitly assume that the acoustic sound in the baryon-photon plasma propagates until recombination with the same speed as in general relativity. This assumption holds as long as the brane effects are negligible during homogeneous cosmological evolution prior to recombination. Since recombination occurs at high redshift, we expect that all possible brane effects on the BAO prior to recombination can safely be neglected. A comparison of results obtained from the BAO and from the matter power spectrum data for similar surveys using a self-consistent perturbation theory for the braneworlds would give us a good handle on the brane effects prior to recombination.

C. CMB data

It is often the practice in cosmological circles to reduce the full CMB likelihood information to a few background expansion parameters (e.g., as discussed in [39] and [40]). It is possible to compress a large part of the information contained in the CMB power spectrum into just a few numbers: specifically the CMB shift parameter R ([41]), and the angular scale of the sound horizon at last scattering l_A, dependent on the baryon density $\Omega_{0b}h^2$ and the scalar spectral index n_s,

$$R = \sqrt{\Omega_{0m}H_0^2}D_A(z_\star)/c, \tag{30}$$

$$l_A = \pi D_A(z_\star)/r_s(z_\star), \tag{31}$$

where $D_A(z)$ is the comoving angular diameter distance, and $r_s(z)$ the comoving sound horizon at redshift z, where $z_\star$ is the redshift for which the optical depth is unity.

The conservative Planck estimates for these quantities are given as [42] $R = 1.7382 \pm 0.0088$; $l_A = 301.63 \pm 0.15$, at $z_\star = 1089.9$. These numbers are effectively observables and they can be applied to models with either nonzero curvature or a smooth dark energy component [43]. However, it has been shown in [44] that the constraints on these quantities, especially on R, are sensitive to changes in the growth of perturbations. Therefore, as also mentioned in [42], one needs to be careful when using these parameters on modified gravity models which are expected to have very different perturbations to the standard dark energy models. We therefore use these observables, but also show the results without them for comparison. We first use the observables l_A and R separately, fixing $z_\star$, to see how they differ. Then for comparison, as in some recent work on modified gravity ([45]), we also use the Planck 2015 priors on wCDM cosmology and the full polarization data for these parameters, which involve the priors $\{l_A = 301.787 \pm 0.089, R = 1.7492 \pm 0.0049, z_\star = 1089.99 \pm 0.29\}$ and the inverse covariance matrix

$$C^{-1} = \begin{pmatrix} 162.48 & -1529.4 & 2.0688 \\ -1529.4 & 207232 & -2866.8 \\ 2.0688 & -2866.8 & 53.572 \end{pmatrix}.$$

IV. RESULTS

We first study our base braneworld model, namely the spatially flat phantom brane model with no dark radiation (i.e., $\Omega_\kappa = 0$, $\Omega_C = 0$) using various combinations of the different data sets to determine the biases in the observations and to determine which combination of the data to use for the full analysis. In our analyses we find that the parameter Ω_{Λ_b} has negligible effect for all the different scenarios; indeed the constraints on the other parameters are practically the same irrespective of the value of Ω_{Λ_b} in all cases. Therefore, although we mention its best-fit and 1σ error levels, we do not depict it in any of the figures that follow.

A. Low and high-z BAO data

Unlike the SNe data, the BAO data can be affected by the value of of the Hubble parameter, due to the effect on r_d, as illustrated in Fig. 5. We attempt to study the effect of H_0 on both high and low redshift BAO data. For low redshift galaxy BAO data, high values of H_0 lead to correspondingly high values for Ω_{0m}, which would naturally be ruled out by other observations, while for high redshift Lyα BAO data, high values of H_0 lead to slightly lower values of Ω_{0m}. This obvious discrepancy has also been be noted in Fig. 4 of [27] for the ΛCDM model, and for the older SDSS DR11 data. We find here that the new DR12 galaxy data continue to have the same discrepancy with the Lyα data. This has the interesting consequence that, for the galaxy BAO data, high values of H_0 are ruled out simply because they would lead to unacceptably high values of Ω_{0m}, i.e., a high value for the combination $\Omega_{0m}h^2$, which would come into conflict with most other measurements. But for the Lyα BAO data, even for a high value of H_0, the combination $\Omega_{0m}h^2$ would still be acceptable, and ruling out high values of H_0 would rest on other, more direct observations of H_0. This inconsistency may be due to some systematics in the data itself, or a true high redshift effect. First reported in [27] for SDSS DR11, this apparent discrepancy has also recently been studied in [46] for the same data set and it has been claimed that the BAO data at $z > 0.43$ is discrepant with ΛCDM at 2.8σ. Our findings for the SDSS DR12 data set are commensurate with these results and show the about 2.3σ discrepancy between high and low redshift BAO data. Thus, although somewhat mitigated due to the degeneracy with braneworld parameters, the disparity that was seen in the ΛCDM model is not entirely removed in the braneworld model either. This then also raises the question whether one should use all the BAO data available together, or use the galaxy BAO data and Lyα BAO data separately, since there is clearly some tension between them. In this paper, we use the entire BAO data set for final results, while also showing the results for the galaxy and Lyα data separately when required. No assumptions or priors are set on the value of H_0.

We first check the results for the BAO data for the phantom brane scenario, with $\Omega_\kappa = 0$, $\Omega_C = 0$ both at high and low redshifts separately, and in conjunction. The results are shown Fig. 6. We see that both the high and low redshift BAO data appear to favor higher values of H_0 but where the low redshift data also prefer high values for Ω_{0m}, the high redshift data favor lower values for Ω_{0m}. When taken together, constraints are much tighter, and commensurate with other measurements of Ω_{0m}, H_0, due to the tension between the two data sets which rules out a fair part of the parameter space. (One also notes a correlation between H_0 and w_0, with higher values of H_0 being more supportive of a lower, and more phantomlike, value of w_0.) Interestingly, both the low and high redshift BAO data appear to rule out $w_0 = -1$ at 2σ albeit at very high values of H_0. When the two data sets are taken in conjunction, $w_0 = -1$ is allowed at 2σ, as the value of H_0 also becomes low for the total data set. Ω_ℓ can have a fairly wide range of values for both data sets, for differing values of Ω_{0m}. Thus, despite the tension in H_0, the constraining power of the BAO on the braneworld parameters does not change to a large extent for different subsets of the data. For further analysis, we use the entire BAO data set, keeping in mind the tension between the high and low redshift data.

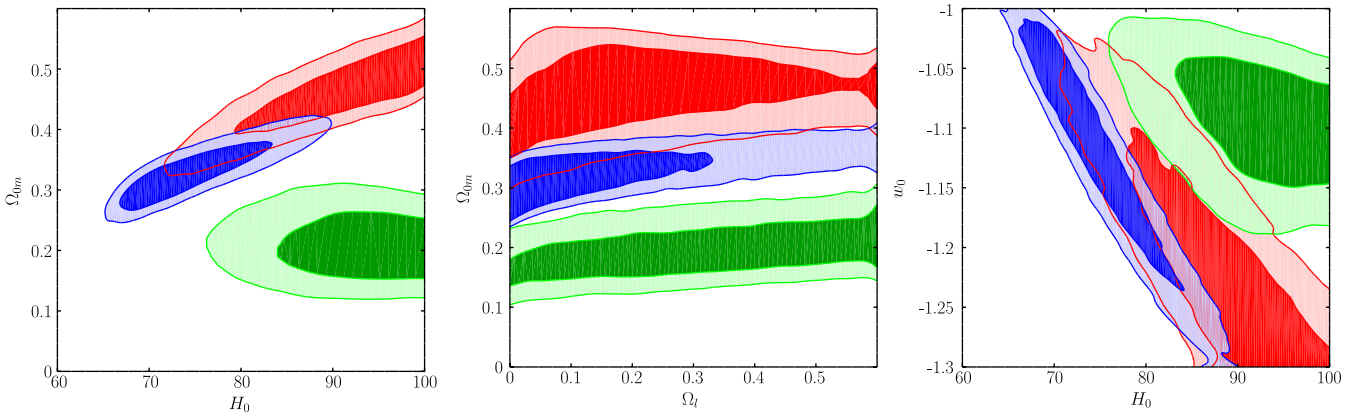

FIG. 6. $1, 2\sigma$ confidence levels in the $\Omega_{0m} - H_0$ (left panel), $\Omega_{0m} - \Omega_\ell$ (middle panel), $w_0 - H_0$ (right panel) parameter space for the base phantom brane with $\Omega_\kappa = 0$, $\Omega_C = 0$, using BAO data. The blue contours represent results for the full BAO data, the red contours those for low-z galaxy data only, and the green contours those for the high-z Lyα data only. The high and low-z BAO data are discrepant at 2σ.$\Omega_\ell = 0$ represents ΛCDM.

B. Compressed CMB data

We now look at the compressed CMB data for the base phantom brane scenario, with $\Omega_\kappa = 0$, $\Omega_C = 0$. We use the BAO data in conjunction with the CMB since typically a single CMB data point is not strong enough to constrain parameters. We see in Fig. 7 that the parameters R and l_A give rather different results at 2σ, with R ruling out a much larger portion of the braneworld parameter space than l_A, and also that R prefers slightly lower values of H_0. This also means that l_A allows for more negative values of the effective equation of state today, i.e., $w_0 \ll -1$, as there is a correlation between higher values of H_0 and lower values of w_0. We also see that when using the $\{l_A, R, z_\star\}$ data set, we obtain confidence levels with degeneracies entirely different from either the l_A or R observation, especially in the Ω_{0m}, H_0 parameter space; e.g., these data appear to favor a larger value of Ω_{0m} at lower H_0. This may be simply a pointer to the fact that these quantities as derived from the standard wCDM model are not compatible with the braneworld models for which perturbations have not been considered. As has been mentioned in [5], the compressed data are dependent on the perturbations, and so, for braneworld models which are obviously expected to have very different perturbations than the standard cosmological constant or scalar field scenario, the values quoted may not be ideal for use. R can be especially sensitive to the perturbations. Therefore we do not use the single observation R in further analysis. We do use l_A to better constrain the degeneracies in the parameters, and we alternatively use the $\{l_A, R, z_\star\}$ data; however, we also simultaneously show the results without the compressed CMB data so that one can observe the difference made by this CMB.

C. Analysis of all data sets

In our final analysis of all the three brane scenarios, we now use the Union 2.1 SNeIa data set, the CMB l_A data (or

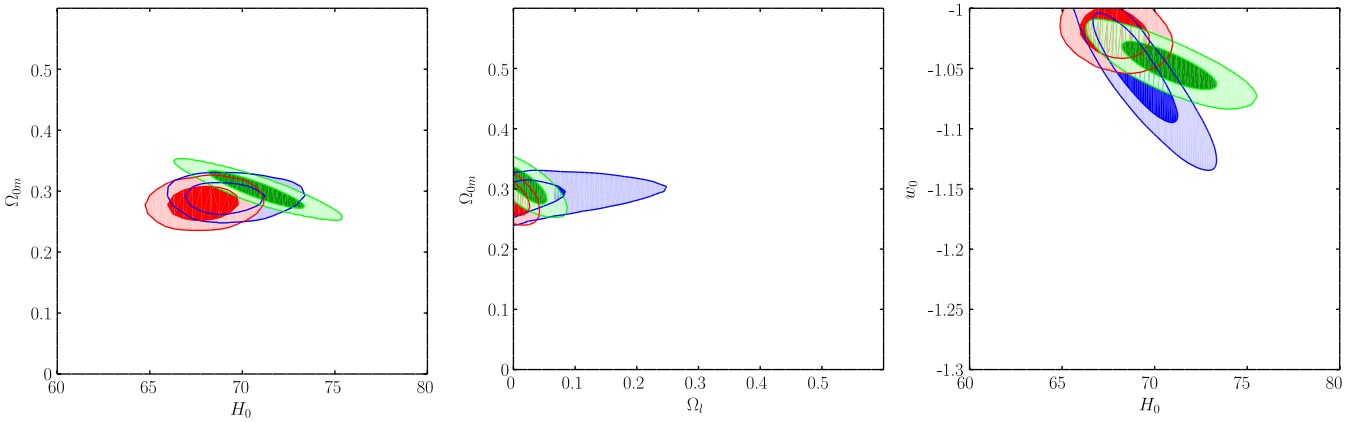

FIG. 7. $1, 2\sigma$ confidence levels in the $\Omega_{0m} - H_0$ (left panel), $\Omega_{0m} - \Omega_\ell$ (middle panel), $w_0 - H_0$ (right panel) parameter space for the base phantom brane with $\Omega_\kappa = 0$, $\Omega_C = 0$, using compressed CMB + BAO data. The red contours represent results for the R parameter, blue contours those for the l_A parameter, and the green contours those for $\{l_A, R, z_\star\}$. $\Omega_\ell = 0$ represents ΛCDM.

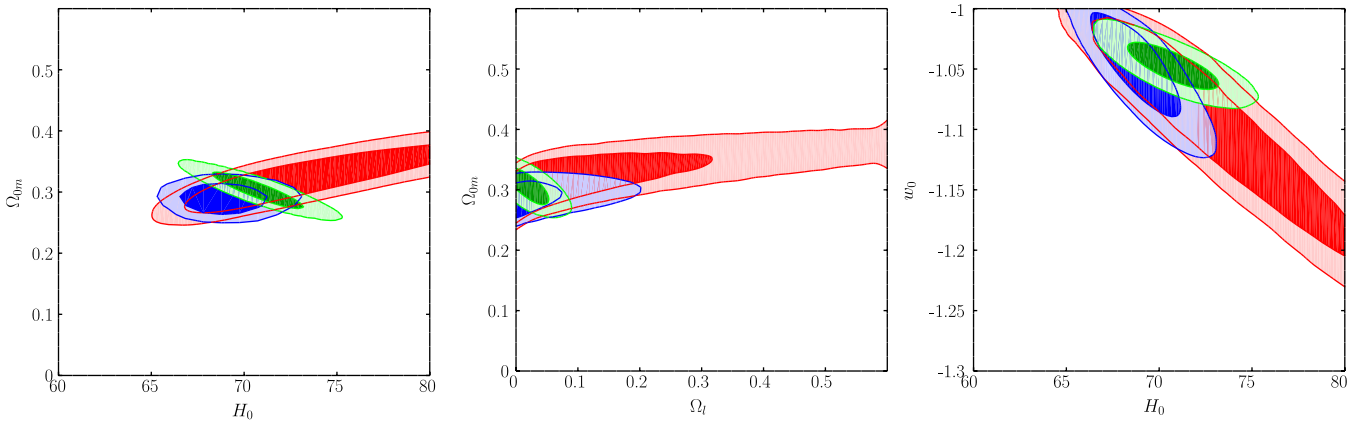

FIG. 8. $1, 2\sigma$ confidence levels in the $\Omega_{0m} - H_0$ (left panel), $\Omega_{0m} - \Omega_\ell$ (middle panel), $w_0 - H_0$ (right panel) parameter space for the base phantom brane with $\Omega_\kappa = 0, \Omega_C = 0$, using SNe Union2.1 + BAO high and low-z data + compressed CMB l_A or $\{l_A, R, z_\star\}$ data. The red contours represent results for just the SNe + BAO data, and the blue contours use l_A in addition, while the green contours use $\{l_A, R, z_\star\}$ in addition. $\Omega_\ell = 0$ represents ΛCDM.

alternatively the $\{l_A, R, z_\star\}$ data), and the full BAO data. For the base phantom brane scenario with $\Omega_\kappa = 0, \Omega_C = 0$, the results are shown in Fig. 8. We see that the presence of the CMB data severely limits the allowed values of the Ω_ℓ parameter. At 1σ, $\Omega_\ell \sim 0.13$ for the SNe + BAO data, while including the CMB l_A data limits $\Omega_\ell \sim 0.08$ at 1σ, while the $\{l_A, R, z_\star\}$ data give the constraints $\Omega_\ell \lesssim 0.05$ at 1σ. The CMB data also put much tighter constraints on the Ω_{0m}, H_0 parameters. In the absence of CMB, the SNe data typically do not in effect constrain these parameters well,

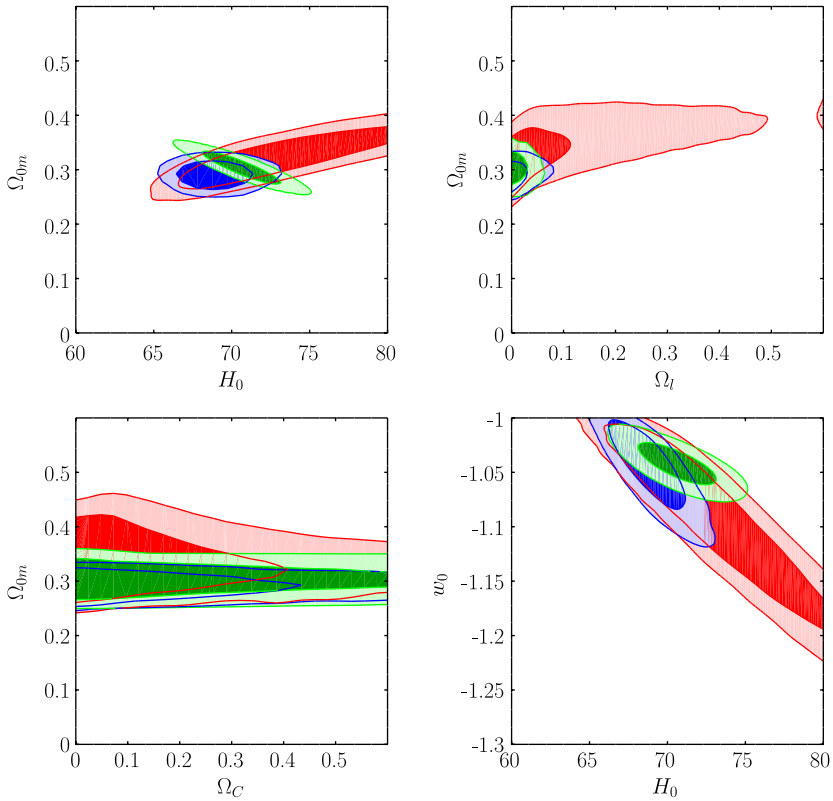

FIG. 9. $1, 2\sigma$ confidence levels in the $\Omega_{0m} - H_0$ (top left panel), $\Omega_{0m} - \Omega_\ell$ (top right panel), $\Omega_{0m} - \Omega_C$ (bottom left panel), $w_0 - H_0$ (bottom right panel) parameter space for phantom brane including dark radiation, using SNe Union2.1 + BAO high and low-z data + compressed CMB l_A or $\{l_A, R, z_\star\}$ data. The red contours represent results for just the SNe + BAO data, and the blue contours use l_A in addition, while the green contours use $\{l_A, R, z_\star\}$ in addition. $\Omega_\ell = 0$ represents ΛCDM.

while the low redshift BAO data, as shown in the previous section, favor somewhat higher values of Ω_{0m} and H_0 than would be allowed by the CMB observations. These values are ruled out when the CMB data point is added, thus tightening the constraints. The higher the values of H_0 allowed, the more the effective equation of state shows phantomlike behavior. Thus the constraints without CMB allow for $w_0 \lesssim -1.19$, for $H_0 \lesssim 78\ \mathrm{km\,s^{-1}\,Mpc^{-1}}$ at 1σ, while the addition of CMB l_A constrains the effective equation of state to $w_0 \simeq -1.09$ and the Hubble parameter to $H_0 \lesssim 71\ \mathrm{km\,s^{-1}\,Mpc^{-1}}$ at 1σ. The CMB $\{l_A, R, z_\star\}$ data constrain $w_0 \lesssim -1.09$ and $H_0 \lesssim 72\ \mathrm{km\,s^{-1}\,Mpc^{-1}}$ at 1σ.

For the case where dark radiation is considered, the results are shown in Fig. 9. In this case we find that the presence of the added Ω_C parameter constrains the Ω_ℓ parameter quite strongly, and Ω_ℓ in this case is smaller than in the previous case. With CMB data, $\Omega_\ell \sim 0.04$ at 1σ, while for just the SNe + BAO data, $\Omega_\ell \sim 0.13$ at 1σ. This is because the term Ω_ℓ is present in two terms in Eq. (3), one positive and the other negative. The best fit in the $\Omega_C = 0$ case holds for some ratio of these two terms. A nonzero Ω_C changes this ratio by increasing the negative, square-rooted term, thus necessitating a corresponding reduction in Ω_ℓ to offset this increase. As previously, the Hubble parameter for the SNe + BAO analysis is allowed to be as high as $H_0 \lesssim 80\ \mathrm{km\,s^{-1}\,Mpc^{-1}}$, and the corresponding effective equation of state is $w_0 \lesssim -1.2$ at 1σ. The addition of CMB l_A constrains the parameters to $H_0 \lesssim 70\ \mathrm{km\,s^{-1}\,Mpc^{-1}}$, $w_0 \lesssim -1.1$ at 1σ, while the addition of $\{l_A, R, z_\star\}$ data gives $w_0 \lesssim -1.08$ and $H_0 \lesssim 72\ \mathrm{km\,s^{-1}\,Mpc^{-1}}$ at 1σ.

The results for the case where the curvature of the Universe is left as a free parameter are shown in Fig. 10. We find in this case that the allowed values of Ω_ℓ for SNe + BAO are roughly the same as in the first case, $\Omega_\ell \sim 0.3$ at 1σ; the addition of a new parameter Ω_κ does not afford much more flexibility in parameter space. In the case where the CMB is considered, given that the CMB is expected to constrain the curvature of the Universe quite strongly, Ω_ℓ is slightly better constrained than the flat case, with $\Omega_\ell \sim 0.08$ at 1σ. However, even with these small values of Ω_ℓ, the curvature of the Universe is allowed to be nonzero, and the Universe at 1σ could either be closed or open, with $-0.5 \lesssim \Omega_\kappa \lesssim 0.5$ even when CMB data are considered. The Hubble parameter is constrained to $H_0 \sim 78\ \mathrm{km\,s^{-1}\,Mpc^{-1}}$, and the effective equation of state to $w_o \sim -1.24$ at 1σ for SNe + BAO data; and the addition of CMB l_A brings these

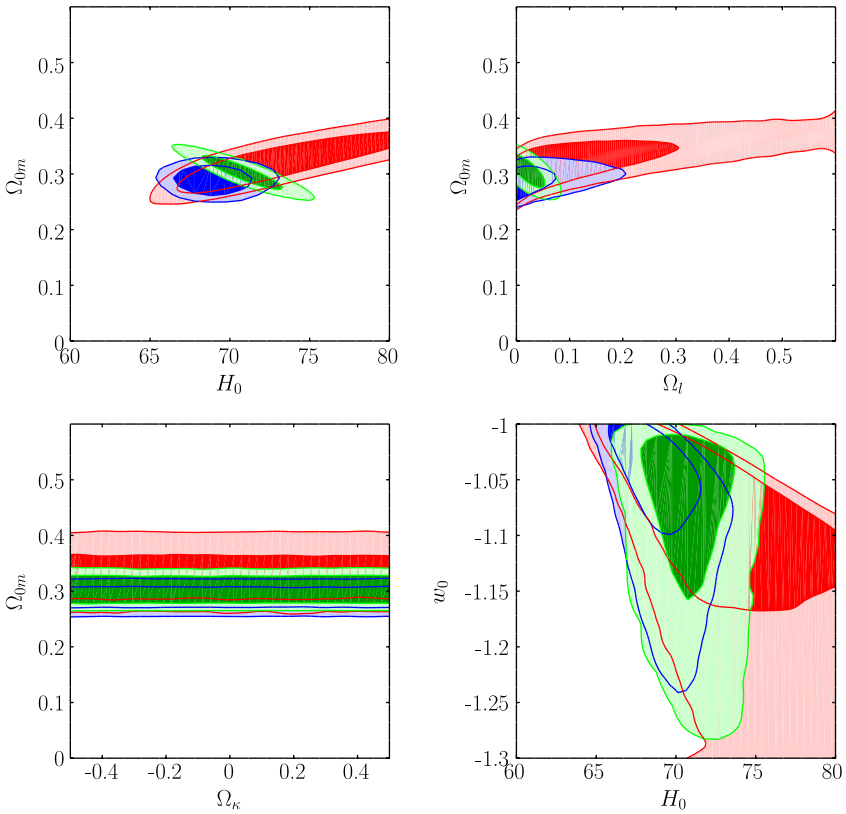

FIG. 10. $1, 2\sigma$ confidence levels in the $\Omega_{0m} - H_0$ (top left panel), $\Omega_{0m} - \Omega_\ell$ (top right panel), $\Omega_{0m} - \Omega_C$ (bottom left panel), $w_0 - H_0$ (bottom right panel) parameter space for phantom brane including curvature, using SNe Union2.1 + BAO high and low-z data + compressed CMB l_A or $\{l_A, R, z_\star\}$ data. The red contours represent results for just the SNe + BAO data, and the blue contours use l_A in addition, while the green contours use $\{l_A, R, z_\star\}$ in addition. $\Omega_\ell = 0$ represents ΛCDM.

TABLE II. Best-fit and 1σ confidence levels on cosmological parameters for various braneworld models for different data sets.

	H_0	w_0	Ω_{0m}	Ω_ℓ	Ω_{Λ_b}	Ω_C	Ω_κ
Phantom brane w l_A	$69.04^{+2.55}_{-1.42}$	$-1.06^{+0.04}_{-0.03}$	$0.289^{+0.010}_{-0.009}$	$0.047^{+0.031}_{-0.047}$	$0.552^{+0.441}_{-0.552}$	...	...
Phantom brane, Ω_C w l_A	$69.02^{+1.44}_{-1.80}$	$-1.05^{+0.04}_{-0.05}$	$0.291^{+0.016}_{-0.010}$	$0.015^{+0.025}_{-0.015}$	$0.537^{+0.461}_{-0.537}$	$0.253^{+0.147}_{-0.253}$	...
Phantom brane, Ω_κ w l_A	$69.06^{+1.42}_{-1.79}$	$-1.07^{+0.09}_{-0.03}$	$0.289^{+0.010}_{-0.009}$	$0.047^{+0.034}_{-0.047}$	$0.552^{+0.439}_{-0.552}$	...	$-0.242^{+0.472}_{-0.207}$
Phantom brane w $\{l_A, R, z_\star\}$	$70.75^{+1.30}_{-1.30}$	$-1.05^{+0.03}_{-0.02}$	$0.303^{+0.011}_{-0.011}$	$0.025^{+0.023}_{-0.025}$	$0.549^{+0.449}_{-0.549}$	...	...
Phantom brane, Ω_C w $\{l_A, R, z_\star\}$	$70.63^{+1.35}_{-1.55}$	$-1.04^{+0.04}_{-0.02}$	$0.304^{+0.013}_{-0.012}$	$0.012^{+0.029}_{-0.012}$	$0.525^{+0.456}_{-0.525}$	$0.265^{+0.315}_{-0.265}$	...
Phantom brane, Ω_κ w $\{l_A, R, z_\star\}$	$70.78^{+2.30}_{-1.43}$	$-1.06^{+0.09}_{-0.04}$	$0.302^{+0.012}_{-0.011}$	$0.045^{+0.032}_{-0.025}$	$0.542^{+0.457}_{-0.542}$	...	$-0.179^{+0.679}_{-0.321}$
Phantom brane w/o CMB	$75.03^{+3.09}_{-7.11}$	$-1.12^{+0.09}_{-0.07}$	$0.332^{+0.032}_{-0.043}$	$0.222^{+0.077}_{-0.222}$	$0.576^{+0.413}_{-0.576}$	...	...
Phantom brane, Ω_C w/o CMB	$75.33^{+4.44}_{-7.67}$	$-1.12^{+0.08}_{-0.08}$	$0.334^{+0.031}_{-0.047}$	$0.098^{+0.031}_{-0.098}$	$0.569^{+0.410}_{-0.569}$	$0.220^{+0.272}_{-0.220}$	...
Phantom brane, Ω_κ w/o CMB	$74.89^{+3.23}_{-7.05}$	$-1.14^{+0.16}_{-0.10}$	$0.331^{+0.031}_{-0.043}$	$0.218^{+0.091}_{-0.218}$	$0.574^{+0.417}_{-0.574}$	...	$-0.185^{+0.423}_{-0.416}$

numbers down to $H_0 \sim 70\ \mathrm{km\,s^{-1}\,Mpc^{-1}}$, $w_0 \sim -1.1$. For the $\{l_A, R, z_\star\}$ data, constraints are weaker, $w_0 \lesssim -1.15$ and $H_0 \lesssim 73\ \mathrm{km\,s^{-1}\,Mpc^{-1}}$ at 1σ.

Table II shows the best-fit and 1σ errors on the various parameters H_0, w_0, Ω_{0m}, Ω_ℓ, Ω_{Λ_b}, Ω_C, Ω_κ in all the cases considered. We note, first of all, that the five-dimensional cosmological constant at 1σ basically encompasses its entire parameter space and also that the results are fairly insensitive to the value of Ω_{Λ_b}. Thus for most such analyses, we may neglect the effects of Ω_{Λ_b}. We note also that without the CMB data, a slightly higher value of Ω_{0m}, H_0, and a lower, more phantomlike w_0, are preferred, and also that the presence of the CMB data puts quite strong constraints on the Ω_ℓ parameter which represents the length scale at which the bulk affects the brane. Using just the SNe and BAO data, we can constrain $\Omega_\ell \sim 0.13$–0.3 at 1σ for the different models. Including the CMB data brings down these numbers to $\Omega_\ell \sim 0.04$–0.10. We also note that, for the case where the restriction on the curvature of the Universe is lifted, even the inclusion of the CMB data does not appear to rule out closed or open universes for braneworld models.

We should be cautious, however, about our interpretation of these results. As we have mentioned in the previous sections, the low and high-z BAO data are discrepant at 2σ; thus results from the joint analysis of both data sets severely constrain the parameter space due to the tension between the data sets. Thus the tight constraints we obtain on the braneworld parameters may very well change as more BAO data become available and this tension between low and high-z data is resolved. We also note that the compressed CMB data may not be completely appropriate to use for modified gravity models. Therefore, the correct way to include the CMB in this analysis would be by doing a complete self-consistent perturbative analysis, rather than using a single number l_A or R or a combination thereof which has been calculated for the Einsteinian gravity framework rather than for modified gravity. The severe constraining of the parameter space thus may be a spurious effect of simply using data inappropriately.

V. CONCLUSIONS

In this work, we have used primarily the SNe type-Ia and BAO observations, as well as compressed CMB data to constrain braneworld parameters. We find that for the analysis using SNe + BAO data, we are faced with some tension between low and high redshift BAO observations, mainly due to their apparently favoring very different values of the Hubble parameter today. Both data sets considered jointly, in conjunction with the SNe allow $\Omega_\ell \lesssim 0.3$ at 1σ for our base phantom brane model with $\Omega_C = 0$, $\Omega_\kappa = 0$. Including the dark radiation term, we find the 1σ constraint of $\Omega_\ell \lesssim 0.13$, $\Omega_C \lesssim 0.4$. For the case where curvature is left to be a free parameter, the results are not very different for Ω_ℓ, but closed and open universes are allowed at 1σ, with $-0.5 \lesssim \Omega_\kappa \lesssim 0.5$. When the compressed CMB data are added, the constraints become much stronger. For the simplest case of phantom brane with $\Omega_C = 0$, $\Omega_\kappa = 0$, using the CMB parameter l_A the Ω_ℓ parameter is constrained at 1σ to $\Omega_\ell \lesssim 0.1$; for the case with dark radiation, we have $\Omega_\ell \lesssim 0.04$, $\Omega_C \lesssim 0.4$, while for the case with nonzero curvature, we obtain $\Omega_\ell \lesssim 0.08$, while the curvature remains as unconstrained as just the SNe + BAO data. When utilizing CMB data, the constraints on the Hubble parameter are naturally very close to the Planck values for ΛCDM, while BAO + SNe data by themselves allow quite higher values for H_0 which are more in line with some direct measurements of H_0. Consequently, the effective equation of state for the SNe + BAO case shows marked phantomlike behavior, with $w_0 \lesssim -1.2$, whereas the addition of CMB constrains it somewhat more, to $w_0 \lesssim -1.1$. We should remember that while the compressed CMB data are ideally suited for use in the cosmological constant or scalar field scenarios, they may not be as suitable for modified gravity, which is expected to have noticeably different perturbations from these scenarios. Therefore, an analysis of the full CMB data with self-consistent perturbations may give entirely different results.

In conclusion, we find that phantom braneworld models are well constrained by current distance measures but by no means ruled out. It is possible to construct braneworld

models compatible with the current observations in which brane-specific effects can cause the acceleration of the cosmological expansion, thus offering a complementary approach to the dark energy problem. We note the discrepancy between high and low-z BAO data and quote the most conservative results using both data sets. Analysis with future BAO data should make it clearer if this inconsistency is in the data itself, or requires a more fundamental change in the cosmological modeling of dark energy. Final constraints on such models can only be obtained if we are able to self-consistently include the perturbative effects of the braneworld models. We note here that perturbations on the braneworld are not expected to modify the transfer function to a great extent, since it is mostly determined by high-z physics which remains similar to the cosmological constant in our model. However, self-consistent perturbations on the brane are expected to affect (i) low-z growth rate through $f(z)$ and σ_8, (ii) the Integrated Sachs Wolfe effect, since Φ differs from the ΛCDM value, and (iii) weak lensing, since $\Phi \neq \Psi$. A companion paper will explore these issues in further detail.

ACKNOWLEDGMENTS

The authors acknowledge useful discussions with Yu. Shtanov and A. Viznyuk. U. A. was supported in this project by the "DST Young Scientist Program" of SERB, India. U. A. also thanks the CHEMCHAM team at IRAP, Toulouse for the use of the hyperion2 cluster for some of the calculations of this paper.

[1] A. G. Riess *et al.*, Astron. J. **116**, 1009 (1998).
[2] S. Perlmutter *et al.*, Astron. J. **517**, 565 (1999).
[3] V. Sahni and A. A. Starobinsky, Int. J. Mod. Phys. D **9**, 373 (2000); P. J E. Peebles and B. Ratra, Rev. Mod. Phys. **75**, 559 (2003); T. Padmanabhan, Phys. Rep. **380**, 235 (2003); V. Sahni, Lect. Notes Phys. **653**, 141 (2004); arXiv:astro-ph/0502032; E. J. Copeland, M. Sami, and S. Tsujikawa, Int. J. Mod. Phys. D **15**, 1753 (2006); J. A. Frieman, M. S. Turner, and D. Huterer, Annu. Rev. Astron. Astrophys. **46**, 385 (2008); R. Durrer and R. Maartens, *Dark Energy: Observational and Theoretical Approaches*, edited by P Ruiz-Lapuente (Cambridge University Press, Cambridge, 2010), pp. 48–91; S. Tsujikawa, arXiv:1004.1493; S. Nojiri and S. D. Odintsov, Phys. Rep. **505**, 59 (2011); T. Clifton, P. G. Ferreira, A. Padilla, and C. Skordis, Phys. Rep. **513**, 1 (2012); M. J. Mortonson, D. H. Weinberg, and M. White, arXiv:1401.0046.
[4] V. Sahni and A. A. Starobinsky, Int. J. Mod. Phys. D **15**, 2105 (2006).
[5] P. A. R. Ade *et al.*, Astron. Astrophys. **594**, A13 (2016).
[6] V. Sahni, A. Shafieloo, and A. A. Starobinsky, Astron. J. **793**, L40 (2014).
[7] T. Sotiriou and V. Faraoni, Rev. Mod. Phys. **82**, 451 (2010); A. de Felice and S. Tsujikawa, Living Rev. Relativ. **13**, 3 (2010); T. Clifton, P. G. Ferreira, A. Padilla, and C. Skordis, Phys. Rep. **513**, 1 (2012); A. Joyce, B. Jain, J, Khoury, and M. Trodden, Phys. Rep. **568**, 1 (2015).
[8] L. Randall and R. Sundrum, Phys. Rev. Lett. **83**, 3370 (1999); Phys. Rev. Lett. **83**, 4690 (1999).
[9] M. K. Mak and T. Harko, Phys. Rev. D **70**, 024010 (2004); S. Pal, S. Bharadwaj, and S. Kar, Phys. Lett. B **609**, 194 (2005); S. Pal and S. Kar, Classical Quantum Gravity **25**, 045003 (2008); T. Harko and K. S. Cheng, Astron. J. **636**, 8 (2006); C. G. Bohmer and T. Harko, Classical Quantum Gravity **24**, 3191 (2007); T. Harko and K. S. Cheng, Phys. Rev. D **76**, 044013 (2007).
[10] Yu. Shtanov and V. Sahni, Phys. Lett. B **557**, 1 (2003).
[11] N. Arkani-Named, S. Dimopoulos, and G. R. Dvali, Phys. Lett. B **429**, 263 (1998); G. Dvali, G. Gabadadze, and M. Porrati, Phys. Lett. B **485**, 208 (2000); G. Dvali and G. Gabadadze, Phys. Rev. D **63**, 065007 (2001).
[12] H. Collins and B. Holdom, Phys. Rev. D **62**, 105009 (2000).
[13] Yu. V. Shtanov, arXiv:hep-th/0005193.
[14] C. Deffayet, Phys. Lett. B **502**, 199 (2001).
[15] V. Sahni and Yu. Shtanov, J. Cosmol. Astropart. Phys. 11 (2003) 014.
[16] V. Sahni and Yu. Shtanov, Phys. Rev. D **71**, 084018 (2005).
[17] Yu. Shtanov and V. Sahni, Classical Quantum Gravity **19**, L101 (2002); V. Sahni and Yu. Shtanov, Int. J. Mod. Phys. D **11**, 1515 (2002); V. Sahni, Yu. Shtanov, and A. Viznyuk, J. Cosmol. Astropart. Phys. 12 (2005) 005; V. Sahni, arXiv:astro-ph/0502032; P. Tretyakov, A. Toporensky, Yu. Shtanov, and V. Sahni, Classical Quantum Gravity **23**, 3259 (2006); Yu. Shtanov, V. Sahni, A. Shafieloo, and A. Toporensky, J. Cosmol. Astropart. Phys. 04 (2009) 023; V. Sahni and Yu. Shtanov, arXiv:0811.3839; A. Viznyuk, Yu. Shtanov, and V. Sahni, Phys. Rev. D **89**, 083523 (2014); S. Bag, A. Viznyuk, Yu. Shtanov, and V. Sahni, J. Cosmol. Astropart. Phys. 07 (2016) 038.
[18] C. Charmousis, R. Gregory, N. Kaloper, and A. Padilla, J. High Energy Phys. 10 (2006) 066; D. Gorbunov, K. Koyama, and S. Sibiryakov, Phys. Rev. D **73**, 044016 (2006); K. Koyama, Classical Quantum Gravity **24**, R231 (2007).
[19] U. Alam and V. Sahni, Phys. Rev. D **73**, 084024 2006.
[20] A. Lue and G. D. Starkman, Phys. Rev. D **70**, 101501 (2004).
[21] A. D. Dolgov, JETP Lett. **41**, 345 (1985); B. Boisseau, G. Esposito-Farese, D. Polarski, and A. A. Starobinsky, Phys. Rev. Lett. **85**, 2236 (2000); R. H. Brandenberger, arXiv:hep-th/0210165; S.-Y. Zhou, E. J. Copeland, and P. M. Saffin, J. Cosmol. Astropart. Phys. 07 (2009) 009; F. Bauer, J. Sola, and H. Stefancic, J. Cosmol. Astropart. Phys. 12 (2010) 029.

[22] V. Sahni, A. Shafieloo, and A. A. Starobinsky, Phys. Rev. D **78**, 103502 (2008); A. Shafieloo, V. Sahni, and A. A. Starobinsky, Phys. Rev. D **86**, 103527 (2012).
[23] V. Sahni, T. D. Saini, A. A. Starobinsky, and U. Alam, JETP Lett. **77**, 201 (2003); U. Alam, V. Sahni, T. D. Saini, and A. A. Starobinsky, Mon. Not. R. Astron. Soc. **344**, 1057 (2003).
[24] A. Shafieloo, U. Alam, V. Sahni, and A. A. Starobinsky, Mon. Not. R. Astron. Soc. **366**, 1081 (2006).
[25] N. Suzuki *et al.*, Astron. J. **746**, 85S (2012).
[26] Betoule *et al.*, Astron. Astrophys. **568**, A22 (2014).
[27] E. Aubourg *et al.*, Phys. Rev. D **92**, 123516 (2015).
[28] T. Delubac *et al.*, Astron. Astrophys. **574**, A59 (2015).
[29] S. Alam *et al.*, arXiv:1607.03155 [Mon. Not. R. Astron. Soc. (to be published)].
[30] R. Jimenez and A. Loeb, Astron. J. **573**, 37 (2002); M. Moresco *et al.*, J. Cosmol. Astropart. Phys. 8 (2012) 006; O. Farooq and B. Ratra, Astron. J. **766**, L7 (2013); M. Moresco *et al.*, arXiv:1601.01701.
[31] L. Samushia and B. Ratra, Astrophys. J. **714**, 1347 (2010).
[32] A. G. Riess, L. Macri, S. Casertano, H. Lampeitl, H. C. Ferguson, A. V. Filippenko, S. W. Jha, W. Li, and R. Chornock, Astron. J. **730**, 119 (2011).
[33] G. Efstathiou, Mon. Not. R. Astron. Soc. **440**, 1138 (2014).
[34] A. Riess *et al.*, Astrophys. J. **826**, 56 (2016).
[35] V. Bonvin *et al.*, arXiv:1607.01790 [Mon. Not. R. Astron. Soc. (to be published)].
[36] G. A. Tammann and B. Reindl, Astron. Astrophys. **549**, A136 (2013).
[37] Y. Chen, S. Kumar, and B. Ratra, arXiv:1606.07316 [Astrophys. J.(to be published)].
[38] M. Moresco, R. Jimenez, L. Verde, A. Cimatti, L. Pozzetti, C. Maraston, and D. Thomas, J. Cosmol. Astropart. Phys. 12 (2016) 039.
[39] A. Kosowsky, M. Milosavljevic, and R. Jimenez, Phys. Rev. D **66**, 063007 (2002).
[40] Y. Wang and P. Mukherjee, Phys. Rev. D **76**, 103533 (2007).
[41] G. Efstathiou and J. Bond, Mon. Not. R. Astron. Soc. **304**, 75 (1999).
[42] P. A. R. Ade *et al.*, Astron. Astrophys. **594**, A14 (2016).
[43] P. Mukherjee, M. Kunz, D. Parkinson, and Y. Wang, Phys. Rev. D **78**, 083529 (2008).
[44] M. Kunz, Phys. Rev. D **80**, 123001 (2009).
[45] J. Neveu *et al.*, arXiv:1605.02627 [Astron. Astrophys. (to be published)]; M. A. Garca-Aspeitia *et al.*, arXiv:1609.08220.
[46] J. Evslin, arXiv:1604.02809.